KAGRA Actuator Noise Modeling Report

Yuta Michimura

June 2, 2017

1 Introduction

This report is to summarize the results of actuator noise modeling for the KAGRA suspensions. The modeling was done by using MATLAB Simulink based NoiseBudget script made by Chris Wipf [1].

The main script and the model for the actuator noise modeling are as follows:

- https://granite.phys.s.u-tokyo.ac.jp/svn/LCGT/trunk/kagranoisebudget/Suspensions/run_SAS_NB.m

- https://granite.phys.s.u-tokyo.ac.jp/svn/LCGT/trunk/kagranoisebudget/Suspensions/SAS.slx

You will also need `findNbSVNroot.m`, `myzpk.m`, `plotdobe.m`, and `plotspectrum.m` in the same directroy to run the script.

The main purpose of this modeling is to check if the actuator noise meet the displacement noise requirement set by MIF group, and to check if the feedback signals to the actuators does not saturate DACs. Small actuation efficiency gives less displacement noise, but it requires more feedback voltage. Although this script works similarly for all suspensions, here I plot the example plots mainly for BS (Type-B suspension) in the next section. Results for each suspension is summarized in the following sections.

2 Model

The Simulink model is shown together with the transfer functions and noises used for the simulation.

2.1 Simulink model

The actuator noise Simulink model is shown in Fig. 1. We had to use some tricks to simulate out-of-loop stability and feedback signal with Simulink NoiseBudget blocks, `NbNoiseCal` and `NbNoiseSink`. FlexTf is used for suspension transfer functions (light purple blocks) to use frequency response data (`frd`). Seismic noise from vertical coupling is also included in the model.
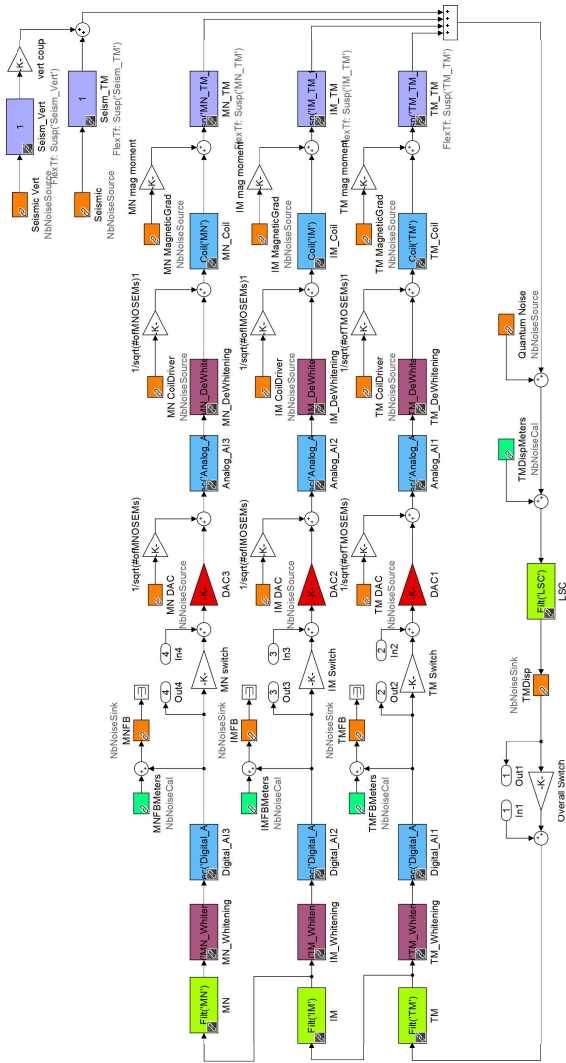
Figure 1: Actuator noise Simulink model.

2.2 Summary of KAGRA Suspensions

KAGRA suspension configurations are summarized graphically in Ref. [2]. For longitudinal degrees of freedom, we basically have actuators for IP (inverted pendulum), IM (intermediate mass), and TM (test mass). For Type-A suspension, we also have actuators for MN (Marionette).

Table 1 is the summary of the actuation for each suspension. Actuation efficiencies for Type-B/Bp coils in N/A are from Ref. [7], those for Type-A coils are from Ref. [5, 6]. Magnets used for Type-A/B/Bp suspensions are SmCo.

Actuation efficiency for a Type-C TM coil are estimated from the measurement done in June 2015 [8]. The measurement for MCe gives 6.9×10^{-6} m/V at DC, and this gives 1.1×10^{-4} N/V assuming IMC mirror mass to be 0.47 kg and the resonant frequency to be 0.94 Hz. The V-I conversion of coil driver for IMC mirrors is 20 mA/V (50 Ω) [9], so this means the actuation efficiency for a Type-C TM coil is 1.4×10^{-3} N/A (this is consistent with Y. Fujii's coil-magnet coupling measurement [10]). Note that magnets for IMC are NdFeB.

Summary of the actuator design can also be found in the wiki below:

- http://gwwiki.icrr.u-tokyo.ac.jp/JGWwiki/KAGRA/Subgroups/VIS/ActuatorDesign

Table 1: KAGRA suspension actuator parameters. The TM/IM masses and wire lengths for Type-B/Bp suspensions come from Ref. [3]. Those for Type-A suspensions come from Ref. [4, 5, 6]. Those for Type-C suspensions come from private communication with K. Arai, R. Takahashi, and T. Saito. TM actuation efficiency for Type-C comes from Ref. [8].

Type	Type-A	Type-B (BS)	Type-B (SR)	Type-Bp	Type-C
Applicable mirrors	ITM,ETM	BS	SRM,SR2,SR3	PRM,PR2,PR3	MCi,MCo,MCe
Mirror diameter	$\phi = 220$ mm	$\phi = 370$ mm	$\phi = 250$ mm	$\phi = 250$ mm	$\phi = 95.95$ mm
Mirror thickness	150 mm	80 mm	100 mm	100 mm	29.5 mm
Mirror substrate	Sapphire	Fused Silica	Fused Silica	Fused Silica	Fused Silica
Mirror mass	22.7 kg	18.9 kg	10.8 kg	10.8 kg	0.47 kg
Intermediate Mass mass	53.2 kg	36.5 kg	15.6 kg	15.6 kg	0.71 kg
Wire length between TM and IM	0.3 m?	0.5 m	0.5 m	0.5 m	0.25 m
Wire length between IM and Platform/BF	0.4 m?	0.5 m	0.5 m	0.5 m	0.25 m
TM magnet size [mm]	$\phi2 \times 2t$	$\phi2 \times 3t$	$\phi2 \times 5t$	$\phi6 \times 3t$	$\phi1 \times 5t$
TM actuation per coil [N/A]	0.0015	0.0138	0.0225	0.129	1.4×10^{-3}
# of TM coils for long.	4	4	4	4	4
IM magnet size [mm]	$\phi2 \times 2t$	$\phi10 \times 10t$	$\phi10 \times 10t$	$\phi10 \times 10t$	N.A.
IM actuation per coil [N/A]	0.015	1.25	1.26	1.26	N.A.
# of IM coils for long.	2	1	1	1	0
MN magnet size [mm]	$\phi5 \times 13t$	N.A.	N.A.	N.A.	N.A.
MN actuation per coil [N/A]	0.45	N.A.	N.A.	N.A.	N.A.
# of MN coils for long.	2	0	0	0	0

2.3 Suspension transfer functions

For the suspension transfer functions, the ones simulated with SUMCON developed by T. Sekiguchi [13] were used.

The example suspension transfer functions from actuation on IM/TM (from respective recoil masses) to TM displacement are shown below.
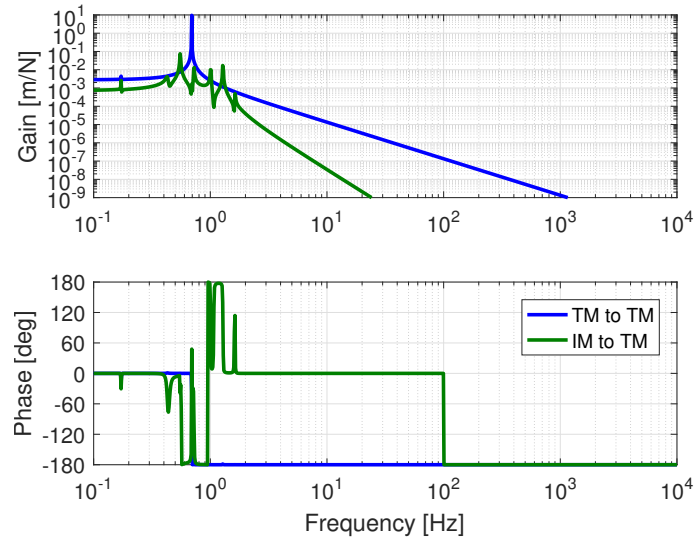

Figure 2: BS suspension transfer functions.

The exmaple seismic noise supression ratio are shown below. The vertical one is also plotted. The vertical to longitudinal coupling was assumed to be 1% in the modeling, for all the suspensions.
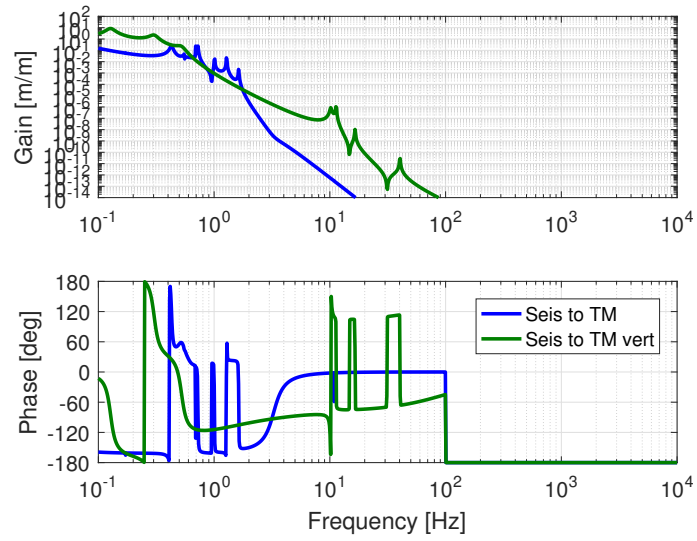
Figure 3: BS seismic noise supression ratio.

2.4 Seismic noise

The Kamioka seismic noise used in the modeling is plotted below. The data is taken on a very noisy day to model the worst case scenario. See Ref. [14] for more detailed seismic noise study.
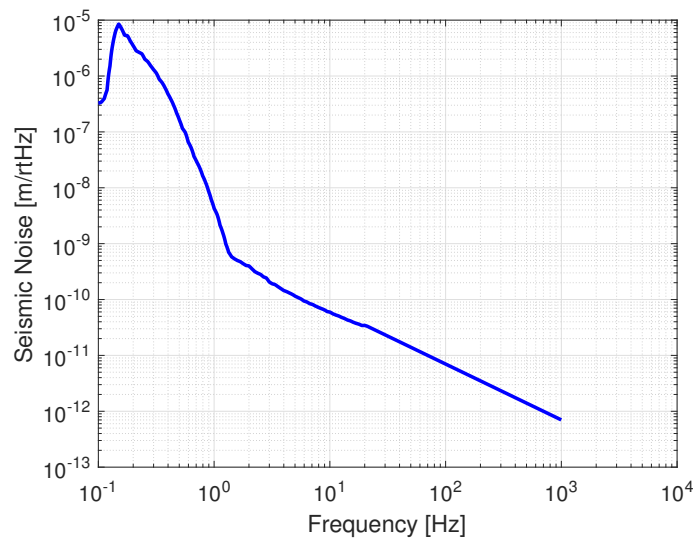
Figure 4: Kamioka seismic noise.

2.5 Coil drivers

We have two types of coil drivers, the high power one and the low power one. They are basically the copies of LIGO-D0902747 and LIGO-D070481, respectively, but have different dewhitening filters compared with LIGO ones. The schematics of the high power coil driver and the low power coil driver are in Ref. [11] and Ref. [12], respectively, and the resistances are 80 Ω for the high power one, and 7.8×10^3 Ω at DC for the low power one. The high power one and the low power one both have switchable three-stage dewhitening filters with pole @ 1 Hz and zero @ 10 Hz (gain of 1 at DC). In the simulation, all the dewhitening filters are turned on.

The low power ones are used for both IM and TM coils for Type-B suspensions, and the high power ones are used for both IM and TM coils for Type-Bp suspensions. V-I conversion factor for the coil drivers when all the dewhitening filters are turned off are plotted in Fig. 5 and Fig. 6. The resistance of the coil is not included here, but it is included in the model (as 13 Ω for Type-B/Bp suspensions).
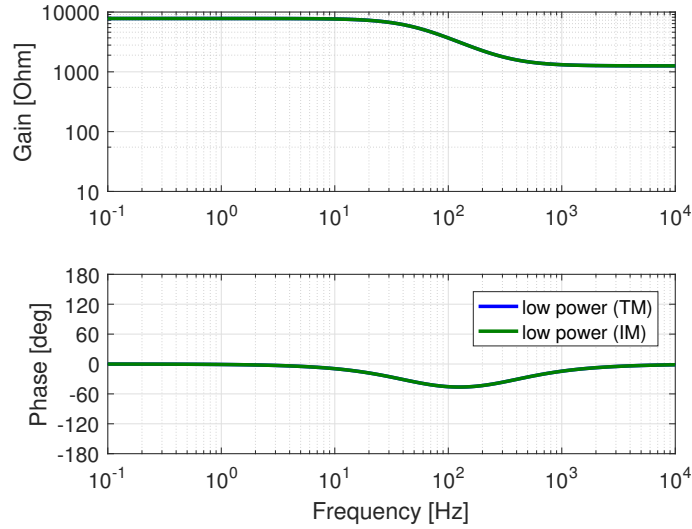
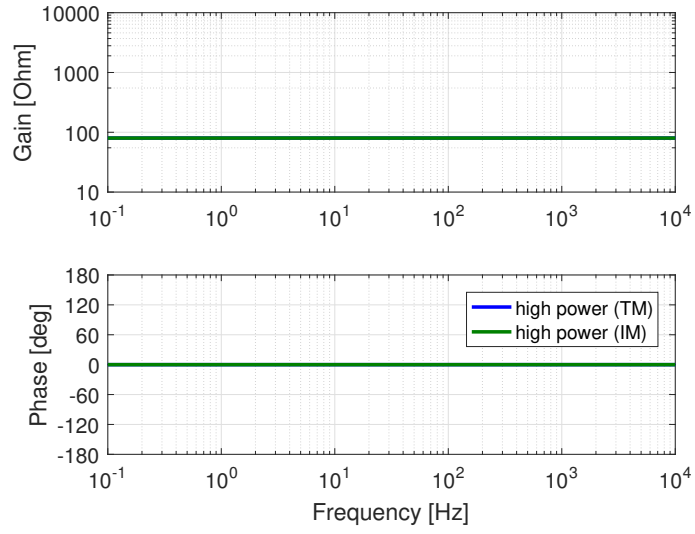Figure 5: Inverse of V-I conversion factors for the low power coil drivers used for Type-B.

7

Figure 6: Inverse of V-I conversion factors for the high power coil drivers used for Type-Bp.

The transfer functions of the whitening and the dewhitening filters are plotted below.
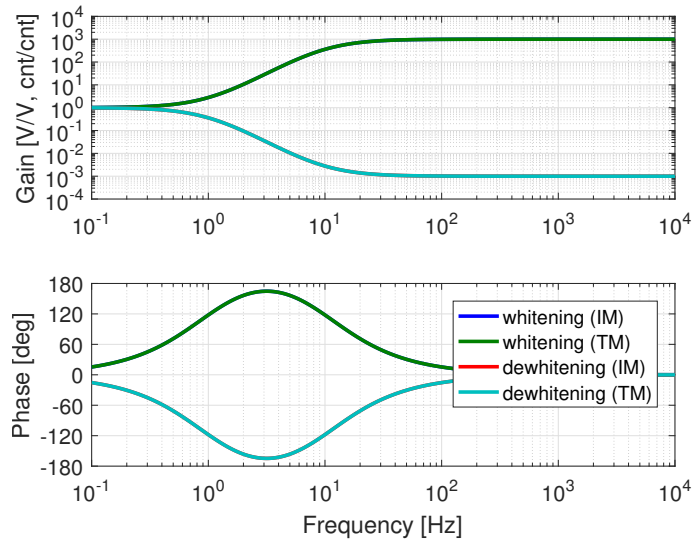

Figure 7: Whitening and dewhitening filters for IM and TM.

Noises of coil drivers used in the model are plotted below, as input equivalent noise to the V-I conversion stage. The spectra come from LIGO-T080014 (high power) and LIGO-T0900233 (low power).
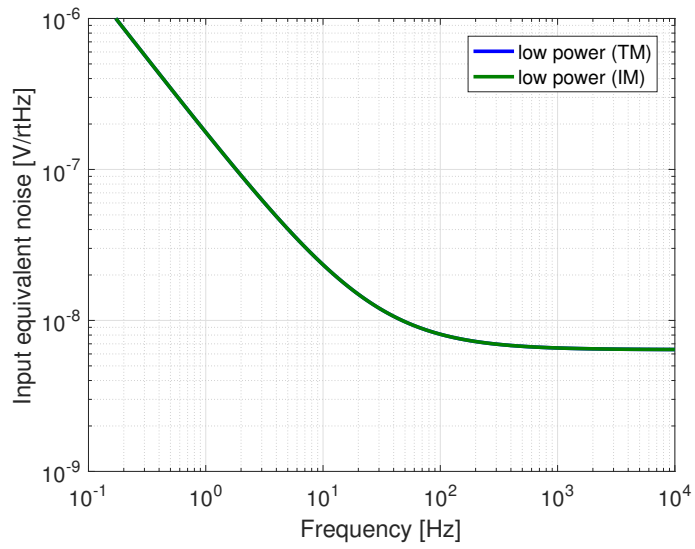
Figure 8: Input equivalent low power coil driver noise spectra.
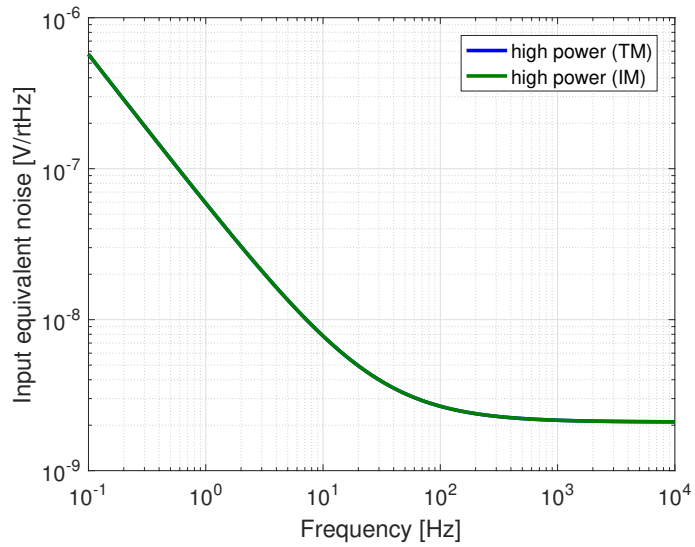
Figure 9: Input equivalent high power coil driver noise spectra.

2.6 DAC

The DAC used for KAGRA is 16 bit and has the range of ± 10 V. So, the least square bit for the DAC is 20 V$/2^{16}$ cnts = 0.305 mV/cnts. The DAC noise is plotted below.
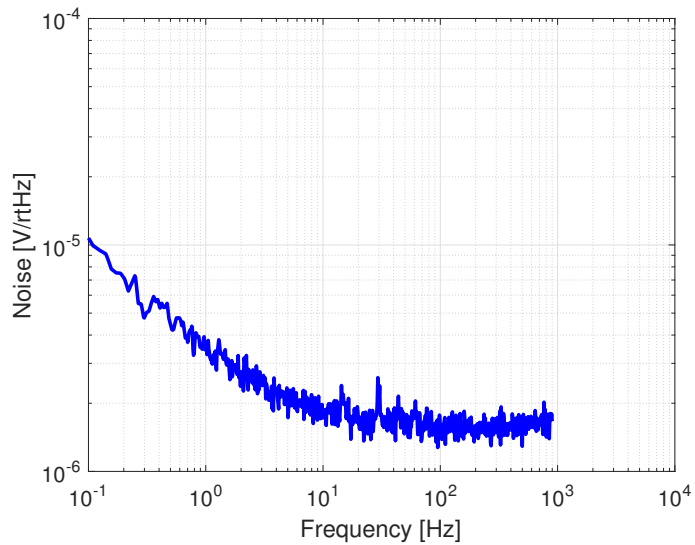
Figure 10: DAC noise.

2.7 Magnetic noise coupling

Magnetic noise calculation method is summarized in Ref. [**?**]. This study shows the force noise from the coupling between the magnetic field gradient and overall magnetic moment of magnets is dominant. So, I included this noise for this modeling.

The magnetic field gradient noise is plotted below. The magnetic field gradient noise is estimated by dividing measured magnetic field noise in Ref. [18] noise by 1 m. Since this noise is measured when there are no equipments installed. Virgo experience show that the magneic noise will be 50 times larger. Detailed measurement inside the cryostat is on going by H. Tanaka.

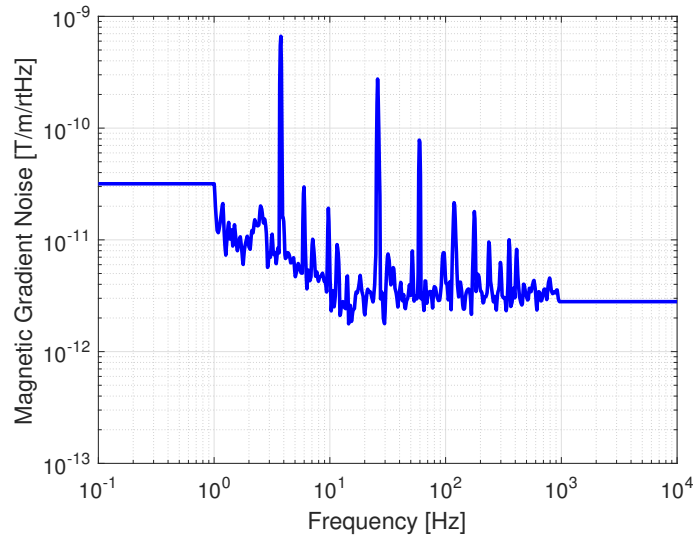Note that the spectrum above 70 Hz and below 0.13 Hz is extrapolated.

Figure 11: Magnetic field gradient noise.

2.8 Quantum noise

The quantum noise incluing the radiation pressure noise and the shot noise is simulated by Optickle by Y. Aso [15]. The simulated quantum noise used in this model is plotted below. DARM is fedback to ETMs, MICH is fedback to BS, PRCL is fedback to PRM, and SRCL is fedback to SRM.
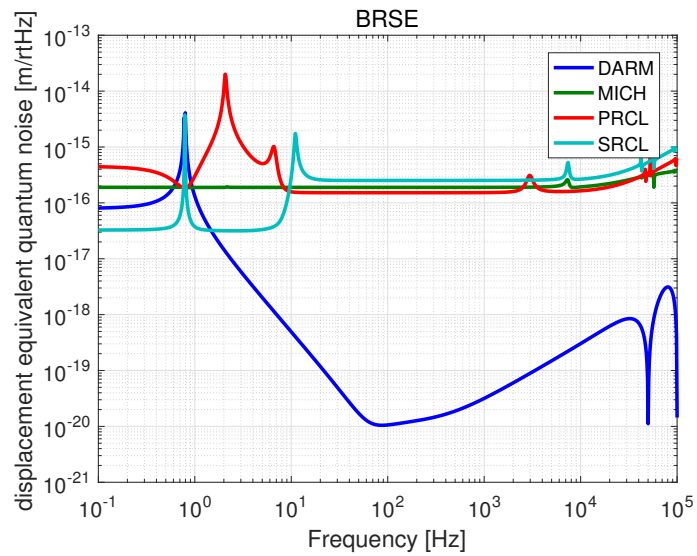

Figure 12: Displacement equivalent quantum noise for BRSE.

3 Results for BS

Resulting plots for BS actuator noise modeling are shown. BS is suspended by a Type-B suspension, but differs from other Type-B's since the mirror mass is heavier.

3.1 Openloop transfer function
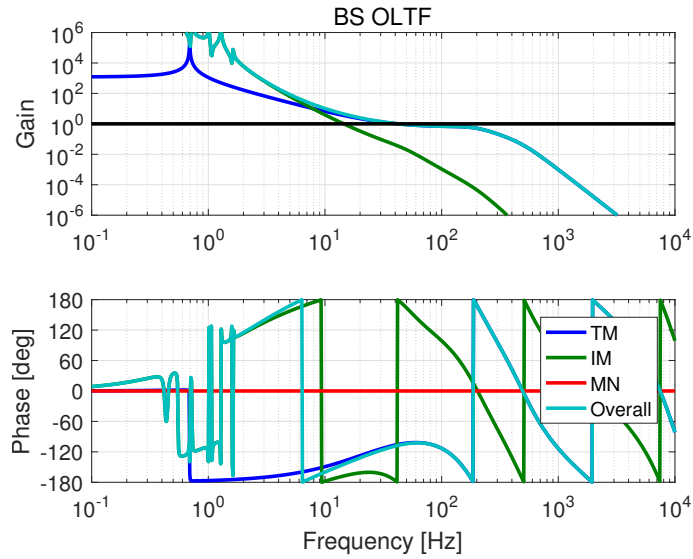
The openloop transfer funtion is shown below.

Figure 13: Openloop transfer functions for the BS length servo.

3.2 Noise budget

The displacement noise budget and the actuator noise budget are shown below. The lines labeled "Requirement" show the BS displacement noise requirement in Ref. [15], and the safety factor of 10 is included. Quantum noise contribution will be subtracted using feedforward technique [15].

As you can see, the seismic noise and the actuator noise meet the requirement above 10 Hz. The magnet size for BS TM was originally 6 mm dia, 3 mm thick, but was changed to 2 mm dia, 3 mm thick to reduce the actuator noise and magnetic noise.
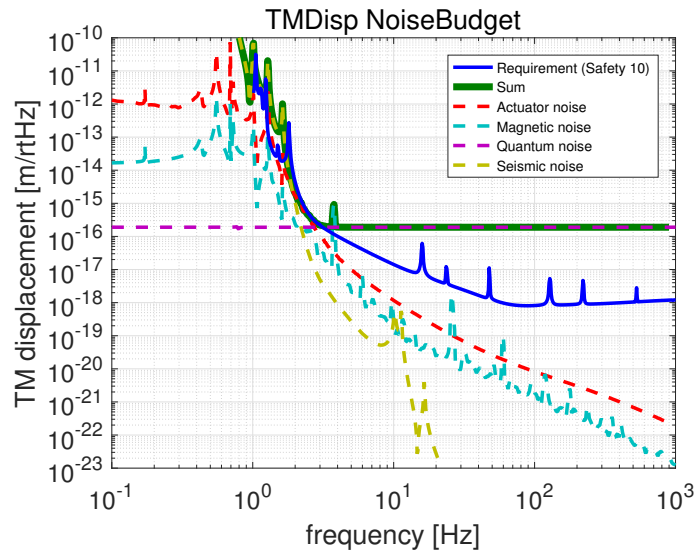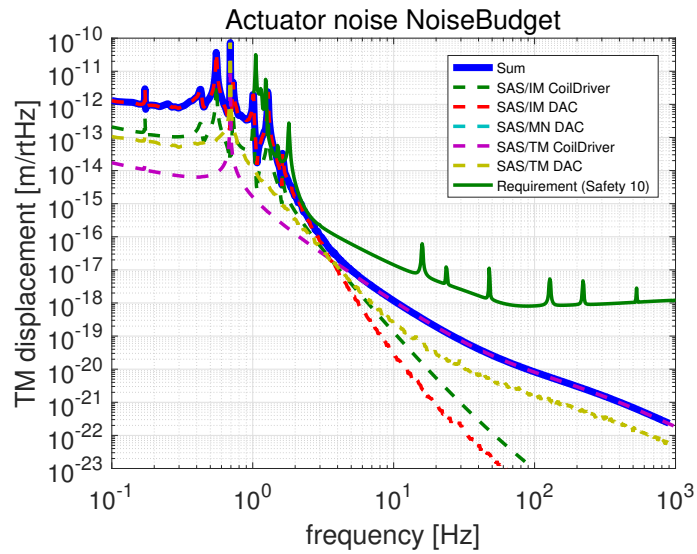
Figure 14: Displacment noise budget for BS.

Figure 15: Actuator noise budget for BS.

3.3 Feedback signal saturation check

The spectra of feedback signals for IM and TM are shown in the figures below. The blue lines labeled "DAC limit" shows the DAC range (2^{16}).

As you can see, the RMS's of the feedback signals do not exceed the DAC limit.
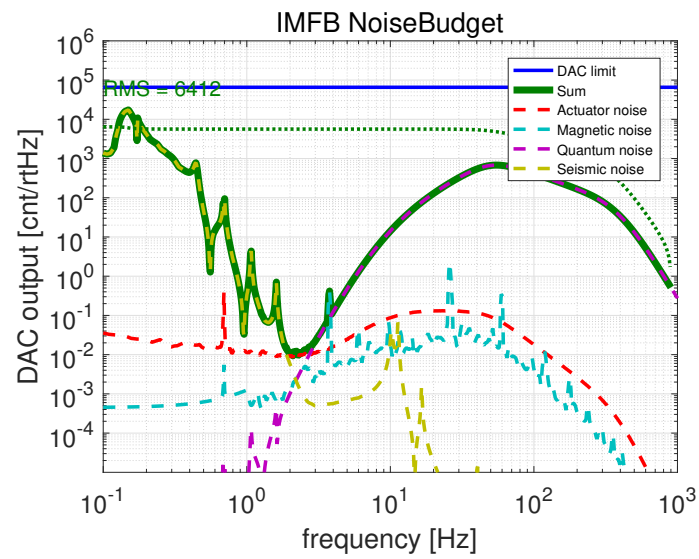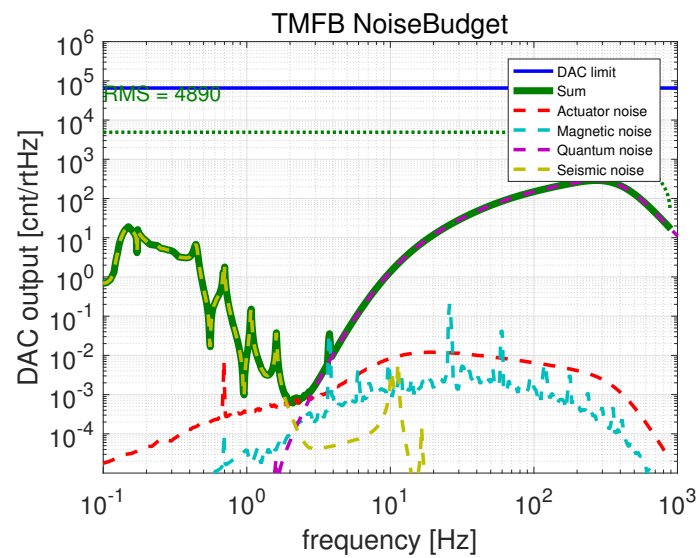
Figure 16: Spectra of feedback signals for the BSIM.

Figure 17: Spectra of feedback signals for the BSTM.

4 Results for SRM

Resulting plots for SRM actuator noise modeling are shown. SRM is suspended by a Type-B suspension. Although displacement noise requirements for SRM and BS is similar, SRM is more severe to the actuator noise since SRM is lighter than BS.

4.1 Noise budget

The displacement noise budget and the actuator noise budget are shown below.

As you can see, the seismic noise and the actuator noise meet the requirement above 10 Hz. Quantum noise contribution will be subtracted using feedforward technique [15]. The magnet size for SRM TM was originally 6 mm dia, 3 mm thick, but was changed to 2 mm dia, 5 mm thick to reduce the actuator noise and magnetic noise.
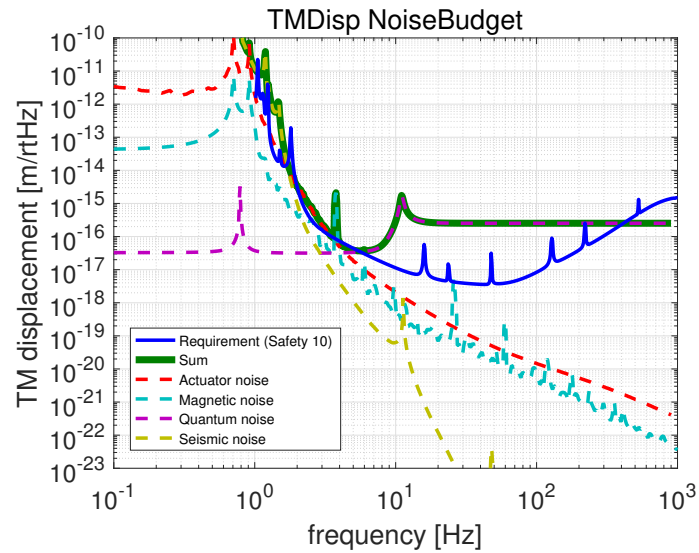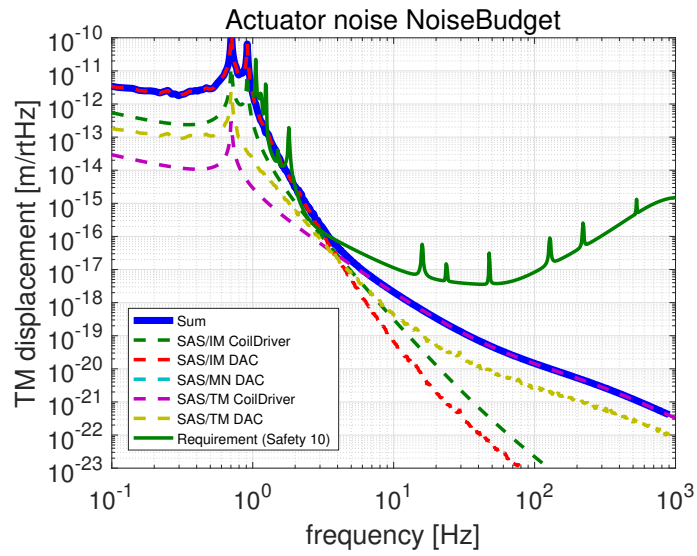

Figure 18: Displacment noise budget for SRM.

Figure 19: Actuator noise budget for SRM.

4.2 Feedback signal saturation check

The spectra of feedback signals for IM and TM are shown in the figures below.
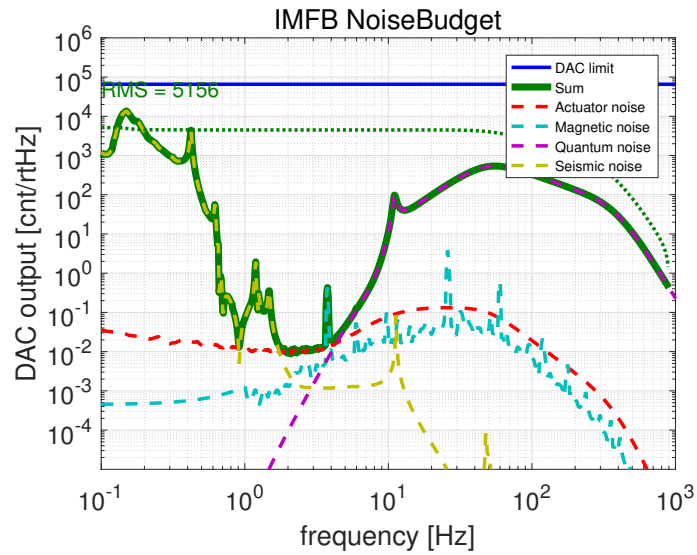As you can see, RMS of the feed back signals do not exceed the DAC limit.

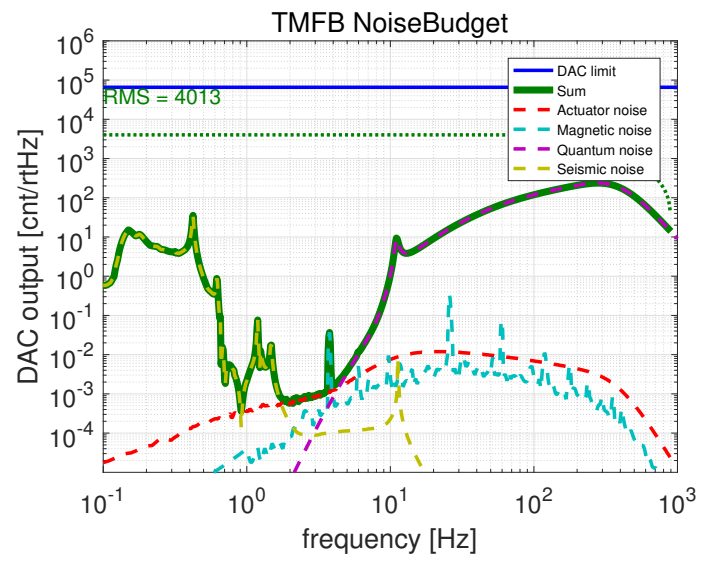Figure 20: Spectra of feedback signals for the SRMIM.

Figure 21: Spectra of feedback signals for the SRMTM.

5 Results for PRM

Resulting plots for PRM actuator noise modeling are shown. PRM is suspended by a Type-Bp suspension. Type-Bp suspension is basically Type-B, but upper stage (Standard Filter) is fixed. So, actuation transfer functions are the same as SRM ones, but seismic suppression ratios are different. To compensate this, high power coil drivers are used instead of low power ones.

5.1 Noise budget

The displacement noise budget and the actuator noise budget are shown below.

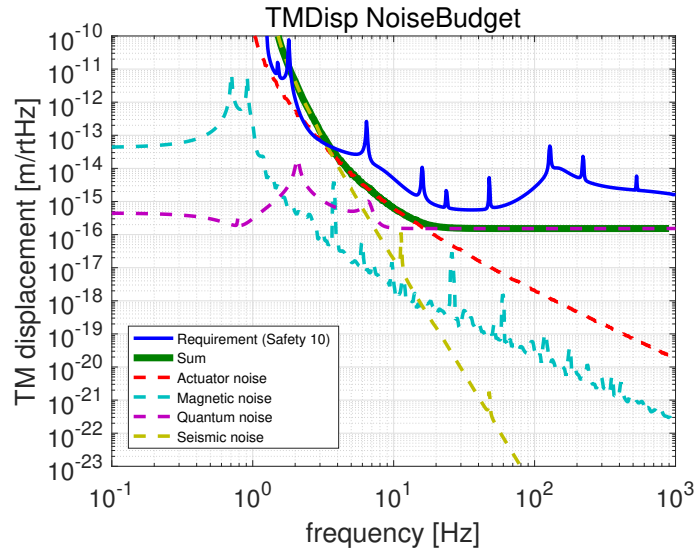As you can see, the seismic noise and the actuator noise meet the requirement above 10 Hz.

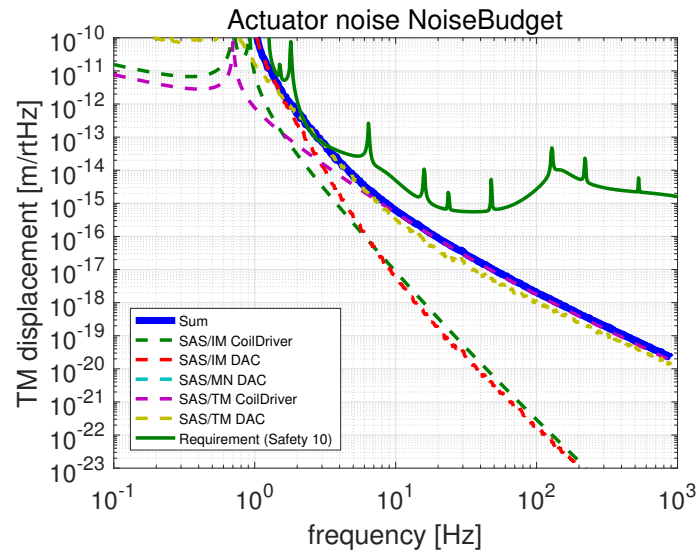Figure 22: Displacment noise budget for PRM.

Figure 23: Actuator noise budget for PRM.

5.2 Feedback signal saturation check

The spectra of feedback signals for IM and TM are shown in the figures below.
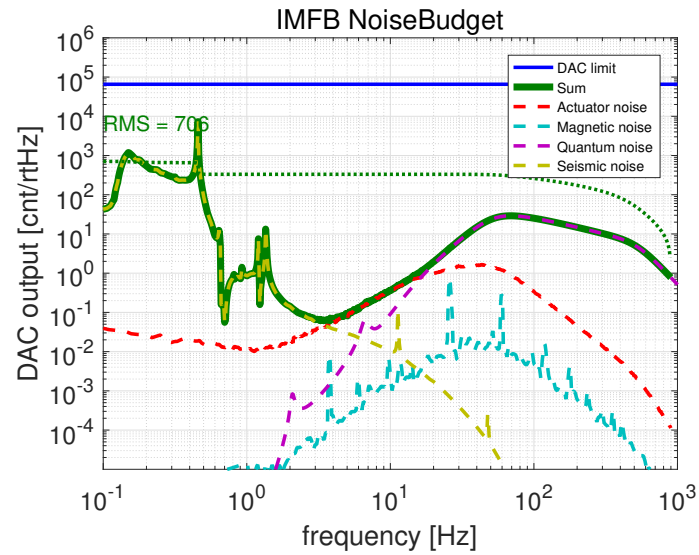As you can see, RMS of the feed back signals do not exceed the DAC limit.

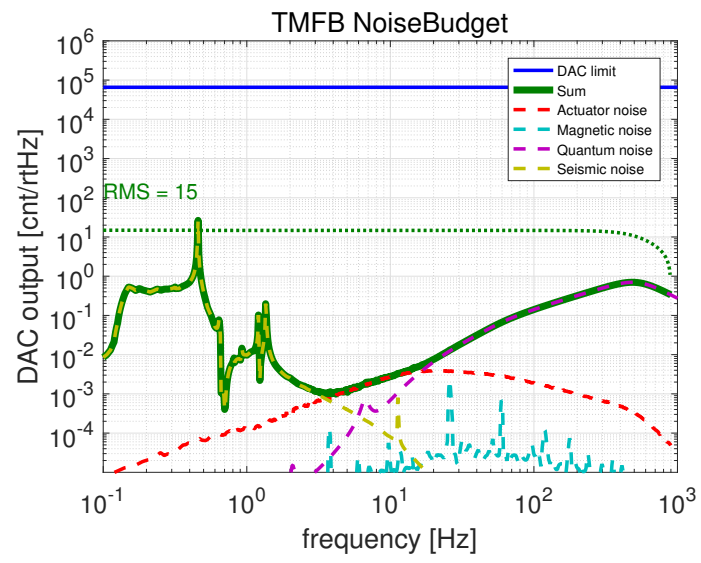Figure 24: Spectra of feedback signals for the PRMIM.

Figure 25: Spectra of feedback signals for the PRMTM.

6 Results for IMC suspensions

Resulting plots for actuator noise modeling for IMC suspensions are shown. IMC mirrors are suspended by Type-C suspension, which is a modified version of the old TAMA PO type suspension. Type-C suspension is a double pendulum fixed on a three-stage stack. There are no actuators for IM. Whitening and dewhitening filters are not used for coils for IMC suspensions. Coil driver for IMC suspensions are different from Type-B/Bp ones; we use TAMA coil drivers described in Ref. [9]. V-I conversion is a flat 50 Ω. We will replace the IMC coil drivers to the high power coil drivers in the future.

For calculating the vertical motion of IMC mirrors, only the isolation ratio from the double pendulum is used in this modeling. The vertical motion should be smaller than the model since we also have isolation from stacks. The vertical to longitudinal coupling was also assumed to be 1%.

6.1 Noise budget

The displacement noise budget and the actuator noise budget are shown below. The displacement noise requirement for the IMC suspensions comes from the frequency noise requirement after the frequency stabilization servo using IMC length.

As you can see, the seismic noise and the actuator noise well meet the requirement above 10 Hz. Quantum noise is calculated assuming input power to IMC to be 100 W.
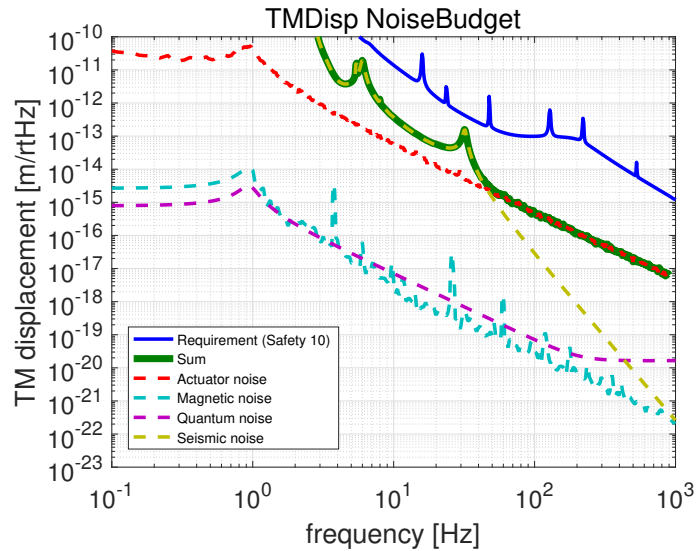

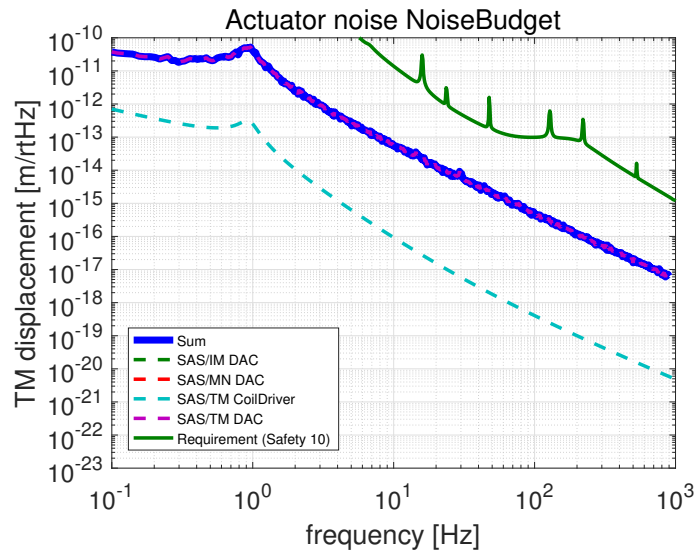Figure 26: Displacment noise budget for IMC.

Figure 27: Actuator noise budget for IMC.

6.2 Feedback signal saturation check

The spectra of feedback signals for IM and TM are shown in the figures below.

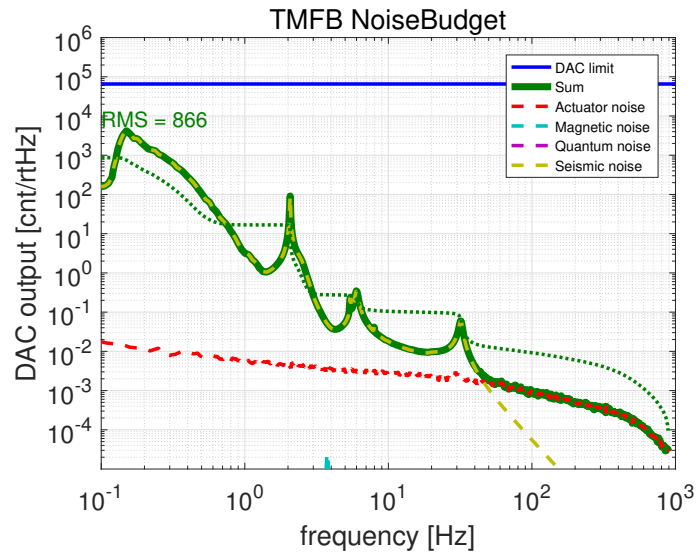As you can see, RMS of the feed back signal does not saturate the DAC limit.

Figure 28: Spectra of feedback signals for the IMCTM.

7 Results for ITM/ETM

Resulting plots for ITM/ETM actuator noise modeling are shown. ITM/ETM is suspended by a Type-A suspension. Low power coil drivers are used for TM, IM, and MN stages. However, for IM and MN stages, modified version is used. R65 and R95 of the driver are modified to be 700 Ω instead of 3.9 kΩ.

7.1 Noise budget

The displacement noise budget and the actuator noise budget are shown below.

As you can see, the seismic noise and the actuator noise meet the requirement above 10 Hz. Quantum noise used here is calculated assuming green locking with input power of 100 mW. This is to check if suspension actuator ranges are sufficient for the green lock. Actually, AOM is used as an actuator for the green lock, but we might also use suspensions for transitioning from the green lock to the IR lock.
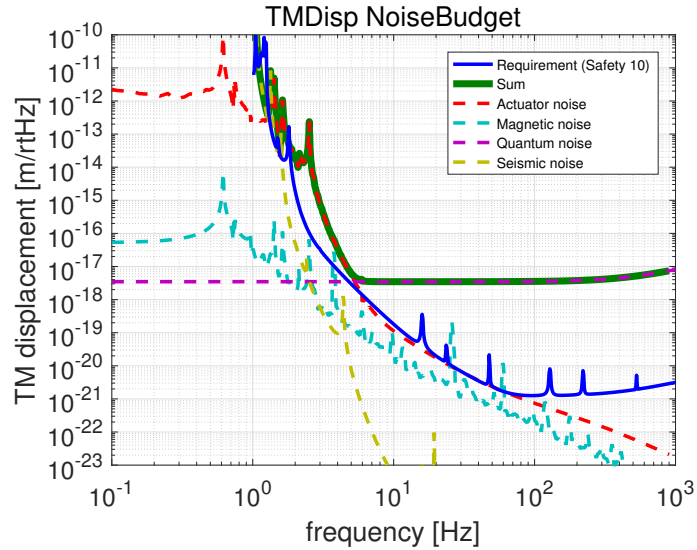

Figure 29: Displacment noise budget for ETM.
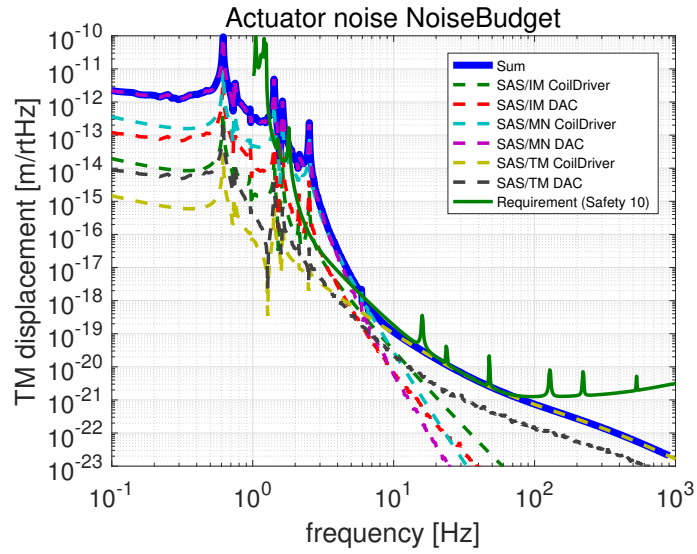
Figure 30: Actuator noise budget for ETM.

7.2 Feedback signal saturation check

The spectra of feedback signals for MN, IM and TM are shown in the figures below.

As you can see, RMS of the feed back signals do not exceed the DAC limit. The magnet size for ETM MN was originally 2 mm dia, 2 mm thick, but was changed to 5 mm dia, 13 mm thick since it saturated the MN DAC. We can further reduce the feedback by implementing damping servo on upper stages.

Figure 31: Spectra of feedback signals for the ETMMN.

Figure 32: Spectra of feedback signals for the ETMIM.

Figure 33: Spectra of feedback signals for the ETMTM.

8   Saturation on lock acquisition

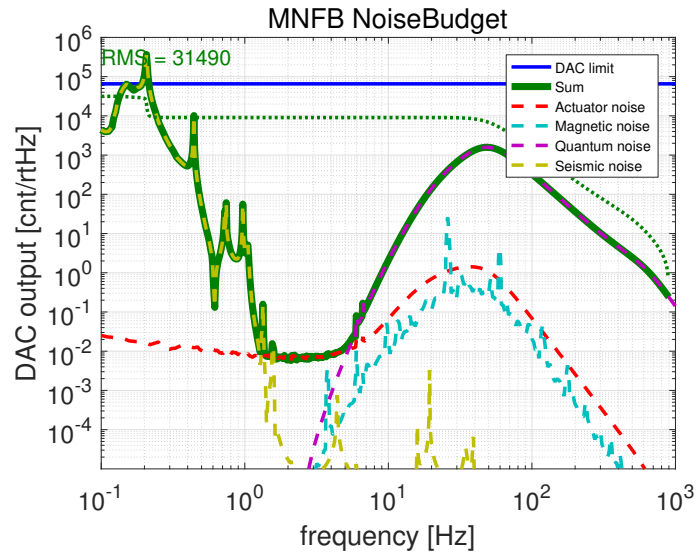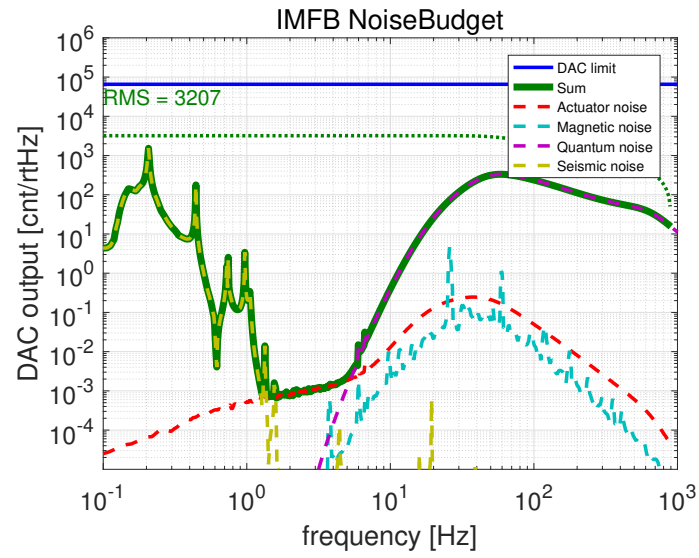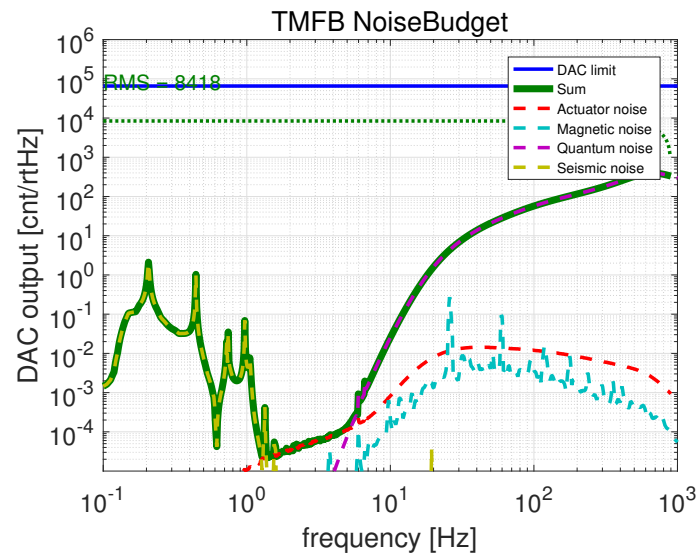We also have to check if the DAC and the coil drivers do not saturate on lock acquisition. The maximum current the low power coil drivers can produce is 10 mA (AD8671) [12], and that for the coil drivers for IMC is 440 mA (EL2099) [9].

The force we need to stop the TM mirror can be roughly estimated by

$$F = \frac{mv}{\Delta t}, \tag{1}$$

where m and v are the mass and the velocity of the mirror, respectively. Δt is the time it takes to pass the linewidth of the error signal d, and $\Delta t = d/v$. So,

$$F = \frac{mv^2}{d}. \tag{2}$$

The estimation for the force and corresponding current to each coil, voltage to each coil driver (DAC output) are show in Table 2.

Table 2: The force we need to stop mirrors. The velocities for Type-B/Bp suspensions are estimated from the RMS velocities after local damping, simulated by A. Shoda. The velocity for Type-C suspension is estimated using the Matlab code from R. Takahashi.

Mirrors	ITM,ETM	BS	SR	PR	IMC
Type	A	B (BS)	B (SR)	Bp	C
Mass [kg]	22.7	18.9	10.8	10.8	0.47
Velocity [um/sec]	TBD	0.2	0.2	4.4	2.3
Linewidth [nm]	9 (green)	532	14	9	1
Force [N]	TBD	1.4e-6	3.1e-5	2.3e-2	2.5e-3
Coil current [mA]	TBD	0.026	0.34	45	443
DAC output [V]	TBD	0.20	2.7	3.6	23

From this study, we can say that;

- We can reduce BS TM actuation efficiency even more if we want to reduce magnetic noise.

- It is desirable to increase number of turns or use bigger magnets for IMC.

9   Summary

- Smaller magnets for BS TM and SRM TM made actuator noise small enough.

- High power coil drivers for PRM IM and TM was OK for actuator noise.

- We can reduce BS TM actuation efficiency even more if we want to reduce magnetic noise.

- It is desirable to increase number of turns or use bigger magnets for IMC.

- Larger magnets for ITM/ETM MN are sufficient for locking.

- Frequency noise should also be included.

References

[1] The source code is available from
https://svn.ligo.caltech.edu/svn/aligonoisebudget.
Some instructions are given at
https://awiki.ligo-wa.caltech.edu/aLIGO/NoiseBudget.

[2] Yuta Michimura: Summary of Suspension Configurations, JGW-D1503415.
http://gwdoc.icrr.u-tokyo.ac.jp/cgi-bin/DocDB/ShowDocument?docid=
3415

[3] Riccardo DeSalvo: Recycler and Beam Splitter suspension structure,
JGW-T1100571.
http://gwdoc.icrr.u-tokyo.ac.jp/cgi-bin/DocDB/ShowDocument?docid=
571

[4] Takanori Sekiguchi: Type-A SAS Mechanical Model Parameters, JGW-
T1302090.
http://gwdoc.icrr.u-tokyo.ac.jp/cgi-bin/DocDB/ShowDocument?docid=
2090

[5] Takahiro Miyamoto: Actuator design of KAGRA cryogenic payload,
JGW-G1605938.
http://gwdoc.icrr.u-tokyo.ac.jp/cgi-bin/private/DocDB/ShowDocument?
docid=5938

[6] Takahiro Miyamoto: status report 20170425, JGW-G1706476.
https://gwdoc.icrr.u-tokyo.ac.jp/cgi-bin/private/DocDB/
ShowDocument?docid=6476

[7] Mark Barton: OSEM Coil/Magnet/Flag Calculation, JGW-T1503239,
Table 1.
http://gwdoc.icrr.u-tokyo.ac.jp/cgi-bin/DocDB/ShowDocument?docid=
3239

[8] Yuta Michimura *et al.*: MCe の並進アクチュエータ伝達関数の測定 (6/25-26)
on IOO blog.
http://gwclio.icrr.u-tokyo.ac.jp/lcgtsubgroup/inoutoptics/2015/06/
mce625-26.html

[9] Gerhard Heinzel: TAMA coil driver modification (2000).
http://tamago.mtk.nao.ac.jp/tama/ifo/general_lib/circuits/000414_coil_
driver/coildrv.pdf

[10] Yoshinori Fujii: coil-magnet coupling measurement, JGW-T1503605.
http://gwdoc.icrr.u-tokyo.ac.jp/cgi-bin/private/DocDB/ShowDocument?
docid=3605

[11] Masahiro Kamiizumi: High Power Coil Driver Board, JGW-D1503503.
http://gwdoc.icrr.u-tokyo.ac.jp/cgi-bin/private/DocDB/ShowDocument?
docid=3503

[12] Masahiro Kamiizumi: Low Power Coil Driver Board, JGW-D1503507.
http://gwdoc.icrr.u-tokyo.ac.jp/cgi-bin/private/DocDB/ShowDocument?
docid=3507

[13] The SUMCON is available from the KAGRA SVN;
https://granite.phys.s.u-tokyo.ac.jp/svn/LCGT/trunk/VIS/sumcon

[14] Takanori Sekiguchi: Seismic Spectrum in Kamioka Mine, JGW-T1402971.
http://gwdoc.icrr.u-tokyo.ac.jp/cgi-bin/DocDB/ShowDocument?docid=2971

[15] Yoichi Aso, Yuta Michimura, Kentaro Somiya: KAGRA Main Interferometer Design Document, JGW-T1200913, Figure 4.1 and 4.2.
http://gwdoc.icrr.u-tokyo.ac.jp/cgi-bin/DocDB/ShowDocument?docid=913

[16] Kenji Ono: Evaluation of BS and RM noise arisen from the AC component of geomagnetism field, JGW-T1503469.
http://gwdoc.icrr.u-tokyo.ac.jp/cgi-bin/DocDB/ShowDocument?docid=3469

[17] Tomofumi Shimoda: Magnetic noise calculation for BS (and ETM/ITM, PRM/SRM), JGW-T1504459.
http://gwdoc.icrr.u-tokyo.ac.jp/cgi-bin/DocDB/ShowDocument?docid=4459

[18] Sho Atsuta: Measurement of Schumann Resonance, JGW-G1605544. http://gwdoc.icrr.u-tokyo.ac.jp/cgi-bin/DocDB/ShowDocument?docid=5544